Author Manuscript
Author Manuscript
Author Manuscript
Author Manuscript

HHS Public Access
Author manuscript
Mod Pathol. Author manuscript; available in PMC 2023 January 06.

Published in final edited form as:
Mod Pathol. 2022 March ; 35(3): 333–343. doi:10.1038/s41379-021-00896-6.

Germline and sporadic mTOR pathway mutations in low-grade oncocytic tumor of the kidney

Payal Kapur, MD[1,2,3,*], **Ming Gao, PhD**[3,4,*], **Hua Zhong, PhD**[1,5,*], **Suneetha Chintalapati, MD**[1], **Midori Mitui, PhD**[1], **Spencer Barnes, BS**[5], **Qinbo Zhou, PhD**[6], **Jeffrey Miyata, BS**[3,4], **Deyssy Carrillo, BS**[3,4], **Venkat Malladi, MS**[3,5], **Dinesh Rakheja, MD**[1,3], **Ivan Pedrosa, MD, PhD**[3,7], **Lin Xu, PhD**[6], **Lisa Kinch, PhD**[6], **James Brugarolas, MD, PhD**[3,4]

[1]Department of Pathology, University of Texas Southwestern Medical Center, Dallas, TX, 75390

[2]Department of Urology, University of Texas Southwestern Medical Center, Dallas, TX, 75390

[3]Kidney Cancer Program at Simmons Comprehensive Cancer Center, University of Texas Southwestern Medical Center, Dallas, TX, 75390

[4]Department of Hematology-Oncology Division of Internal Medicine, University of Texas Southwestern Medical Center, Dallas, TX, 75390

[5]Department of Bioinformatics, University of Texas Southwestern Medical Center, Dallas, TX, 75390

[6]Department of Population and Data Sciences, University of Texas Southwestern Medical Center, Dallas, TX, 75390

[7]Department of Radiology, University of Texas Southwestern Medical Center, Dallas, TX, 75390

Abstract

Low-grade Oncocytic Tumor (LOT) of the kidney is a recently described entity with poorly understood pathogenesis. Using next-generation sequencing (NGS) and complementary approaches, we provide insight into its biology. We describe 22 LOT corresponding to 7 patients presenting with a median age of 75 years (range 63–86 years) and male to female ratio 2:5. All 22 tumors demonstrated prototypical microscopic features. Tumors were well circumscribed and solid. They were composed of sheets of tumor cells in compact nests. Tumor cells had eosinophilic cytoplasm, round to oval nuclei (without nuclear membrane irregularities), focal subtle perinuclear halos and occasional binucleation. Sharply delineated edematous stromal islands were often observed. Tumor cells were positive for PAX8, negative for CD117 and exhibited diffuse and strong cytokeratin-7 expression. Six patients presented with pT1 tumors and at a median follow-up of 29 months, 4 patients were alive without recurrence (3 patients had died from unrelated causes). All tumors were originally classified as chromophobe renal cell carcinoma, eosinophilic variant

Author of correspondence: Payal Kapur, MD, Professor, Kidney Cancer Program, Department of Pathology, University of Texas Southwestern Medical Center, 5323 Harry Hines Blvd., Phone: 214-633-6363, Fax: 214-633-8817, payal.kapur@utsouthwestern.edu, &, James Brugarolas, MD, PhD, Professor, Kidney Cancer Program, Department of Internal Medicine, Hematology-Oncology Division, University of Texas Southwestern Medical Center, 5323 Harry Hines Blvd., Phone: 214-648-4059, Fax: 214-648-1960, james.brugarolas@utsouthwestern.edu.
*contributed equally to this study

Conflicts of interest disclosures: The authors declare that they have no conflict of interest.

Author Manuscript Author Manuscript Author Manuscript Author Manuscript

(chRCC-eo). While none of the patients presented with known syndromic features, one patient with multiple bilateral LOTs was subsequently found to have a likely pathogenic germline *TSC1* mutation. Somatic, likely activating, mutations in *MTOR* and *RHEB* were identified in all other evaluable LOTs. As assessed by phospho-S6 and phospho-4E-BP1, mTOR complex 1 (mTORC1) was activated across all cases but to different extent. *MTOR* mutant LOT typically exhibited lower levels of mTORC1 activation, possibly related to mTORC1 dimerization and the preservation of a wild-type *MTOR* copy (retained chromosome 1). Supporting its distinction from related entities, gene expression analyses showed that LOT clustered separately from classic chRCC, chRCC-eo and RO. In summary, converging mTORC1 pathway mutations, mTORC1 complex activation and a distinctive gene expression signature along with characteristic phenotypic features support LOT designation as a distinct entity with both syndromic and non-syndromic cases associated with an indolent course.

Keywords

Oncocytoma; eosinophilic variant of chromophobe renal cell carcinoma; RCC with cytoplasmic eosinophilia; eosinophilic tumor; unclassified oncocytic tumor; hybrid oncocytic / chromophobe RCCs; LOT; low-grade oncocytic tumor; TSC associated RCC

Introduction

The differential diagnosis of renal tumors with exclusively eosinophilic (or oncocytic) cytoplasm traditionally involves differentiating a malignant tumor, chromophobe renal cell carcinoma (chRCC), in particular the eosinophilic variant (chRCC-eo), from benign renal oncocytoma (RO)[1,2]. This distinction frequently poses a dilemma given their shared morphologic features especially with unifocal tumors in non-syndromic settings[2]. Furthermore, markers often used in the differential diagnosis, such as cytokeratin (CK) 7 (typically diffuse in chRCC and scattered in RO), are not always able to distinguish chRCC-eo, which can have rare or patchy expression. This difficulty is further compounded by a lack of definite criteria to distinguish chRCC-eo from the classic variant of chRCC.

The differential diagnosis of renal tumors with eosinophilic cytoplasm has become even more challenging with newly described entities[2,3]. These include tuberous sclerosis complex (TSC) associated renal cell carcinoma (RCC)[4,5], hybrid oncocytic/chromophobe tumors (HOCT) in the setting of Birt-Hogg-Dubé (BHD) syndrome[6], eosinophilic solid and cystic RCC (ESC RCC)[7–9], MiT family translocation RCC[10,11], succinate dehydrogenase (SDH)-deficient RCC[12], fumarate hydratase (FH)-deficient RCC[13], eosinophilic vacuolated tumors (EVT)/ RCC with eosinophilic and vacuolated cytoplasm[14–17], as well as other currently unclassified RCCs[18].

Recently, a distinct low-grade oncocytic tumor (LOT) was reported as a potential new entity[19,20]. Two publications describe LOT as unifocal small tumors (mean size 3.9 cm [range 1.1–13.5 cm]), devoid of aggressive features in non-syndromic settings[19,21]. Histologically, LOT have a predominantly solid architecture composed of tight nests with foci of delineated edematous stroma that contains strands of tumor cells. The tumor cells have eosinophilic/oncocytic cytoplasm, uniform round nuclei without significant

Author Manuscript Author Manuscript Author Manuscript Author Manuscript

irregularities, and only focal subtle perinuclear halos. They have a characteristic but unexpected immunoprofile: they are CD117 (c-kit) negative and show strong and diffuse CK7 reactivity. To date, all tumors have been reported to be associated with an indolent clinical course[2,19,20,22].

We previously published a comprehensive genomic analysis of 167 primary non-clear cell RCC that included RO (n= 31), renal oncocytic neoplasm (RON) (n= 5), and chRCC (36 classic variant; 12 eosinophilic variant)[23]. Notably, the majority of chRCC-eo lacked characteristic DNA copy number alterations of the classic variant of chRCC. Two of the 12 chRCC-eo morphologically fit the description of LOT[19,20,24] and were CD117 negative/CK7 positive. Interestingly, both tumors had a unique gene expression signature, and harbored mammalian target of rapamycin (*MTOR*) mutations. These results led us to hypothesize that LOT may be characterized by a unique gene expression signature and mutations of the mammalian target of rapamycin complex 1 (mTORC1) pathway (such as in *MTOR, TSC1, TSC2* or *RHEB*). In the current study, we evaluate this notion through systematic analyses of eosinophilic tumors at our institution that fit the morphology and immunohistochemistry profiles of LOT.

Materials and methods

Case selection

The study was conducted with approval by the UT Southwestern Medical Center (UTSW) Institutional Review Board (IRB) and according to the Health Insurance Portability and Accountability Act (HIPAA) guidelines. We searched our institutional RCC database (Kidney Cancer Explorer [KCE]; sponsored by the UT Southwestern [UTSW] Kidney Cancer NIH SPORE grant, the Lyda Hill Department of Bioinformatics and the Bioinformatics Core Facility) for tumors diagnosed as chRCC, RON, and RO. We excluded diagnoses based on biopsy specimens as well as consultation cases. Between 2005 and 2016, 204 cases (99 chRCC, 20 RON, and 85 RO) were identified out of a total of 1870 renal tumors, including some that were published previously[23]. Archival material, where available, was retrieved (204 cases) and re-reviewed by two genitourinary (GU) pathologists (S.C and P.K), who classified these tumors as LOT based on previously described characteristic morphology and IHC (CK7 diffuse+/CD117−)[19]. Additional IHCs were obtained as needed during review (CK7 and CD117, CK20, cathepsin K, TFEB [transcription factor EB], TFE3 [transcription factor E3], SDHB [succinate-dehydrogenase B], and FH [fumarate hydratase]).

Clinical Data

Patient age at nephrectomy, race, sex, tumor size, AJCC TNM staging categories, histologic subtype, date of surgery, date of development of metastases, and date of last follow-up were collected from KCE. The tumors were staged based on the 2018 American Joint Committee on Cancer (AJCC) TNM classification for pathologic staging. Data in KCE were complemented through comprehensive review of clinical data and pathology slides.

Author Manuscript Author Manuscript Author Manuscript Author Manuscript

Immunohistochemistry

IHC analysis was performed on representative 3–5 μm formalin-fixed paraffin-embedded (FFPE) whole tumor tissue sections. Staining for routinely used markers including Pax8 (10336-1-A P, 1:1000; Proteintech), CA9 (11071-1-AP, 1:100; Thermo Fisher), CD10 (56C6, 1:40; Dako), CK7 (M7018- OV-TL 12/30, 1:100; Dako), CK20 (7019-Ks20.8, 1:50; Dako), CD117 (A4502, 1:700; Dako), Melan A (7196-A103, 1;200; Dako), cathepsin-K (37259-3F9, 1:100; Abcam), FH (100743-J13, 1:1500; Santa Cruz), SDHB (14714-21A11, 1:100; Abcam), TFE3 (MRQ-37, 1:200; Cell Marque), TFEB (166736, 1:100; Santa Cruz), vimentin (M0725, 1:75; Dako), phospho-S6 (Ser240/244) (p-S6) (5364-D68F8, 1:300; Cell Signaling Technology) and phospho-4E-BP1 (Thr37/46) (p-4EBP1) (236B4, 1:800; Cell Signaling Technology) was performed using a Dako automated system (Agilent).

Immunoreactivity was interpreted as “negative” if < 5% tumor cells stained positively. P-S6 and p-4EBP1 expression was determined based on the percentage of tumor cells staining positive and the intensity of expression, which were multiplied.

Next generation sequencing

All hematoxylin and eosin (H&E) FFPE slides were examined to select most representative areas from 7 LOTs as well as matched normal tissues. Corresponding areas were macrodissected (LOT 3–7). Tissue was submitted to BGI Genomics for DNA extraction and whole-exome sequencing (WES). DNA libraries were sequenced to an average read depth > 100x for exome sequencing using 2 × 75-base paired-end on a HiSeq2500 platform (Illumina, San Diego, CA, USA). DNA from LOT 7 tumor and LOT 6 normal did not pass quality control. The two index cases (LOT 1–2) were previously evaluated using fresh frozen tissue with simultaneous extraction of both DNA and RNA to enable integrative genomic analyses[25] and sequencing was performed as described previously[23].

Sanger Sequencing

Validation of the *MTOR, TSC1, RHEB* mutations was carried out using PCR followed by Sanger sequencing on an ABI 3700. 20ng of patient DNA from normal and tumor samples was amplified using primers designed to capture each of the mutations in LOT 3–6. Normal tissue from LOT 6 had not passed quality control and more tissue was not available for further analysis. Oligonucleotide primer sequences are available on request.

Molecular analysis

Exome-seq reads from FASTQ files were aligned to the human reference genome GRCh38 (hg38) using the Burrows-Wheeler Aligner algorithm (BWA-MEM; version 0.7.17) set to default parameters[26]. BAM files were generated using Picard Tools (version 2.20.5) to add read group information and sambamba was used to mark PCR duplicates. GATK toolkit (version 4.0.7)[27–29] was used to perform base quality score recalibration and local realignment around indels. MuTect2[30], VarScan (v2.4.0)[31], Shimmer (v0.2)[32], SpeedSeq (v0.1.2)[33], Manta (v1.6.0), and Strelka2 (v2.9.10)[34] were used to call somatic variants and small-scale insertions and deletions (indels) for each tumor. A mutation that was repeatedly called by any two of these software tools was retained. Annovar was used to annotate germline/somatic mutations and indels[35]. A minimum of 7 total reads in the normal

Author Manuscript Author Manuscript Author Manuscript Author Manuscript

sample and at least 3 variant reads in the tumor sample with a variant allele frequency (VAF) ≥ 5% were required for somatic mutation calling. Intronic, untranslated region and intergenic mutations outside splice sites were filtered out. Missense mutations predicted to be benign by both PolyPhen-2 and SIFT (with < 5% chance of inducing functional changes at the protein level) were filtered out[36]. Somatic variant calls were inspected using Integrated Genomics Viewer v2.3.4 (IGV; Broad Institute, MIT Harvard, Cambridge, MA, USA). Variants were classified according to the American College of Medical Genetics and Genomics (ACMG) 2015 Guidelines. COSMIC and ClinVar were used as additional databases to annotate cancer relevance and clinical potential for detected variants.

We carried out somatic copy number variation (CNV) analyses on our exome-seq data using CNVkit (https://github.com/etal/cnvkit) with default parameters on tumor-normal pairs. CNVkit uses both on- and off-target sequencing reads to calculate $\log_2$ copy ratios across the genome for each sample and improves accuracy in copy number calling by applying a series of corrections[37]. Arm gain or loss was called when > 50% of the chromosome exhibited copy number gain or loss[38].

RNA-seq reads were aligned to the human reference genome GRCh38 (hg38) using STAR[39] with the parameters "--runThreadN 48 --outSAMtype BAM Unsorted --outReandsUnmapped Fastx." The FeatureCounts[40] software program with parameters "--primary -O -t exon -g transcript_id -s 0 -T 48 --largestOverlap --minOverlap 3 --ignoreDup -p -P -B –C" was used to measure gene expression levels. The human genome annotation file employed by FeatureCounts was downloaded from the UCSC table browser under the RefSeq Gene track. Genes were kept if they had at least 10 read counts in one or more of the 141 samples evaluated (2 LOT, 35 RO [including 4 RON-favor RO], 9 chRCC-eo [including 1 RON-favor chRCC-eo], 35 classic chRCC, and 60 normal kidney). These data were integrated with 89 TCGA cases (4 LOT, 15 chRCC-eo, 46 classic chRCC, and 24 normal kidney samples) for downstream analyses. Two tumor/normal RO pairs believed to have tumor/normal labels transposed were removed from the gene expression analyses: sample 13730N, which was labeled as a normal and had a non-coding mutation [chrM:564:G->A] previously reported to occur in RO[41] and its corresponding tumor (13730T), which lacked the mutation); and sample XP174N, which had a frameshift insertion [chrM:11866:A->AC] on *MT-ND4* also reported in RO[41] and its corresponding tumor (XP174T), which lacked the mutation. The Bioconductor packages edgeR[42] (version 3.28.1) and sva (version 3.34.0) were employed to perform normalization (using TMM[43]) and batch effect removal (using ComBat[44]). EdgeR was further utilized to: (1) identify differentially expressed genes between LOT and chRCC-eo types, and (2) perform KEGG analysis of differentially expressed genes to identify significantly enriched pathways with p-values ≤ 0.05.

Results

Study Cohort

From among 204 cases between 2005 – 2016 of chRCC, RON, and RO at our institution with adequate material, we identified 22 tumors corresponded to 8 nephrectomy/partial nephrectomy cases and 7 patients that fit the morphologic description of LOT. Overall, LOT represented 4% (8 of 204 cases) of reviewed cases and 0.4% of all nephrectomies for renal

Author Manuscript Author Manuscript Author Manuscript Author Manuscript

tumors at our institution during the study timeframe. All 22 tumors had been originally diagnosed as chRCC-eo.

Baseline Clinical Characteristics and Clinical Course

The patient demographics and tumor characteristics are summarized in Table 1. The patients ranged from 63 to 86 years at diagnosis (mean age: 75 years). There were more females than males (M:F ratio, 2:5). None of the patients had prior documented history of a syndrome including TSC and BHD. Suspicious skin lesions, pneumothoraxes, unexplained seizures, angiomyolipomas, or other characteristic syndromic features were not documented. Three patients, however, had multiple renal masses. One patient (LOT 3) had multiple bilateral renal tumors (6 on the right and 10 on the left) (Supplementary Figure 1A–B). The patient was found to have a likely pathogenic germline variant in the *TSC1* gene. The patient received therapy with an mTORC1 inhibitor, everolimus, which led to remission of several lesions and stabilization of the rest. Another patient (LOT 5) had a history of prior nephrectomy for a benign renal tumor at an outside institution, and another (LOT 7) was found to have a concurrent contralateral 2nd renal mass. Neither LOT 5, nor LOT 7, were found to have a genetic predisposition. Amongst the solitary LOTs, there was predilection for the right kidney (right: 5; left: 1). Most patients underwent partial nephrectomy. At the time of this analysis, 3 patients were deceased due to unrelated causes including LOT 1, who expired from a subsequently diagnosed contralateral metastatic clear cell RCC. The 4 remaining patients were alive with no evidence of metastatic disease at the time of last follow-up. Follow-up ranged from 3 months to 53 months (median 29 months).

Imaging Features

Computed tomography (CT) was available in 4 patients (LOT 1–4). All masses exhibited areas with intense enhancement (i.e. similar to that of renal cortex) during the corticomedullary phase likely signifying pronounced angiogenesis (Supplementary Figure 1). LOT 3 had multiple bilateral renal masses with similar appearance (Supplementary Figure 1A–B). These tumors also demonstrated irregular areas of decreased central enhancement with some degree of progressive centripetal enhancement during the excretory phase (Supplementary Figure 1B). Renal imaging confirmed the absence of classic angiomyolipoma features (i.e. lacking macroscopic fat) in all cases evaluated.

Pathologic Features

Grossly, the tumors were noted to be well circumscribed, solid, tan to brown, and homogenous on cut surface. Tumors ranged from 0.5 to 7.8 cm in size (mean: 3.1 cm). Areas with loose myxoid stroma, similar to oncocytomas, were appreciated grossly. None of the tumors had renal sinus involvement (Table 1). AJCC pathologic T stage was pT1a in 4/8, pT1b in 3/8, and pT2a in 1/8.

A review of the H&E slides demonstrated striking morphologic similarities in all 22 tumors. All tumors were well demarcated, either devoid of or with a thin partial peripheral fibrous pseudocapsule (Figure 1A). At low power, tumors were homogenous and solid. They were composed of sheets of compact uniform small nests (Figure 1A–B). Abrupt areas of hypocellular, loose edematous stroma with scattered cords of tumor cells were

Author Manuscript Author Manuscript Author Manuscript Author Manuscript

present (Figure 1C). In some tumors, focal areas of hemorrhage and dilated vascular channels filled with serous or hemorrhagic fluid were also seen (Figure 1D). The tumor cells were uniform, polygonal in shape and had ill-defined cell borders (Figure 1E). They contained eosinophilic, finely granular, cytoplasm and central round to mildly oval nuclei with focal mild nuclear membrane irregularities and prominent small eosinophilic nucleoli (Figure 1E–F). Subtle perinuclear clearing, mild pleomorphism and binucleation were seen in all cases, more apparent focally in some cases. Focal scattered small clusters of lymphocytes and histocytes were also seen (generally near the loose stromal areas) (Figure 1F). Tumor necrosis, frequent or atypical mitosis, nuclear pleomorphism, cytoplasmic clearing, cytoplasmic stippling or inclusions were not identified. Typical features of classic chRCC (wrinkled, raisinoid, nuclear membrane; marked perinuclear clearing; well defined cell borders; clear cytoplasm) were not apparent. Peritumoral blood vessels were markedly thick-walled in the majority of cases (Supplementary Figure 2A). All 16 tumors in the patient with the germline *TSC1* mutation (LOT 3) showed similar features with the addition of small tumorlets in the adjacent renal parenchyma (Supplementary Figure 2B). Consistent with the imaging findings, no angiomyolipomas were identified in adjacent kidney sections. A small distinct area (3.0 mm) with slightly different morphology was observed in one of the 16 tumors with large intracytoplasmic vacuoles similar to EVT (Supplementary Figure 2C–D). A small distinctive area (4.0 mm) was also seen in a LOT 4 tumor with more pronounced perinuclear clearing and nuclear membrane irregularities (Supplementary Figure 2E–F).

Immunohistochemical Features

LOTs (including representative sections from multiple tumors in LOT 3) were interrogated with immunohistochemical (IHC) stains. All LOTs showed diffuse and strongly reactive cytokeratin 7 and were negative for CD117 (Table 2, Figure 1G–H). They were positive for PAX8, retained FH as well as SDHB, and were negative for TFE3 and TFEB. They were also negative for HMB45/Melan A, cytokeratin 20, cathepsin K, and carbonic anhydrase-IX. Whenever performed, E-cadherin was positive whereas CD10 and vimentin were negative.

Molecular Features

Whole exome sequencing (WES) was available for 2 cases (LOT 1, 2) from our previously published study[23]. Among the new cases (LOT 3–7), DNA from the tumor region of LOT 7 and normal kidney of LOT 6 did not pass quality control. WES from 5 tumors with paired normal samples demonstrated mutations in mTORC1 pathway genes (*MTOR, TSC1,* or *RHEB*) in all cases (Table 3, Supplementary Figure 3). In addition, unpaired WES analyses from the LOT 6 tumor also showed an *MTOR* gene mutation (Table 3, Supplementary Figure 4A, 5). Variant calls were inspected using the Integrated Genomics Viewer (IGV; Supplementary Figure 4). Mutations were validated by Sanger sequencing on available tumor and normal samples (Supplementary Figure 5).

The presence of mTORC1 pathway gene mutations across all of the samples (LOT 1, 2, 5, 6 [*MTOR*], LOT 3 [*TSC1*] and LOT 4 [*RHEB*]) (Table 3) suggested that mTORC1 may play a role in LOT development. To evaluate this notion further, we assessed the particular mutations. While RHEB and mTOR are positive regulators of mTORC1 and

Author Manuscript Author Manuscript Author Manuscript Author Manuscript

mutations would be expected to be activating, TSC1 is a negative regulator and mutations would be expected to inactivate it. A likely pathogenic germline *TSC1* variant was detected in the blood (and normal kidney sample) from LOT 3. The mutation caused a substitution two nucleotides after exon 15 of the *TSC1* gene (NM_000368.4:c.2208+2T>A), and was predicted to abolish the native splice donor site (Supplementary Figure 4B). In addition, a somatic frameshift TSC1 mutation (p.Arg760Serfs*2) was found in the tumor (Table 3, Supplementary Figure 4A). mTOR mutations were found in LOT 1 (mTOR p.L2427Q), LOT 2 (mTOR p.S2215Y), LOT 5 (mTOR p.S2413L) and LOT 6 (mTOR p.K1452_E1455del). Consistent with their being activating, 3 out of the 4 mTOR mutations affected a residue previously shown to be mutated in other tumors (https://www.cbioportal.org; https://cancer.sanger.ac.uk/cosmic)[45,46]. Furthermore, two mutations (p.L2427Q and p.S2215Y) were previously shown to activate mTORC1 in studies in vitro[45,46,47]. A mutation in RHEB in LOT 4 (RHEB p.Y35L) was both previously reported in other tumors (https://www.cbioportal.org) and shown to be activating in vitro[45].

To evaluate the functional significance of the least characterized mTOR mutations (K1452-E1455 deletion and p.S2413L), we assessed their impact on the mTORC1 structure. We mapped the mutations onto the crystal structures of both the apo and RHEB-activated mTOR proteins (Figure 2A). Previously published cancer-associated mTOR mutations leading to kinase hyperactivation tend to occur at specific areas including the FAT hinge (i.e. A1459P) and the interface between the kinase C-lobe and FAT domain (i.e. E2419K) where they destabilize the apo state[48,49,50]. The K1452-E1455 deletion removes a single turn from a hinge helix in the FAT domain near the known hyperactivating A1459 mutation (Figure 2B left). The turn interacts with neighboring helices that adopt alternate conformations in the inactive and active states and the deletion would remove helical interactions from both states suggesting increased flexibility at the hinge that could lead to hyperactivation. The mTOR p.S2413L mutation resides in the kinase C-lobe at the FAT domain interface. This interface also adopts alternate conformations in the active and inactive states (Figure 2B right). Another known activating mutation (E2419K) is found in the same C-lobe helix at the FAT interface and is thought to lower the barrier to activation[48,50]. Overall, these data are consistent with the notion that the K1452-E1455 deletion and p.S2413L substitution are similarly activating as other previously reported mTOR mutations tested in vitro.

To evaluate the impact of these mutations on mTORC1 activity, we analyzed p-S6 (Ser240/244) and p-4E-BP1 (Thr37/46). All LOTs evaluated showed p-S6 expression in at least 5% tumor cells (Figure 3). Similar results were observed for p-4E-BP1 (Figure 3).

However, we observed a range of mTORC1 activation. Higher activation was observed in LOT 3, 4, and 5, but LOT 1, 2, 6 and 7 had lower levels (Figure 3). These data suggested a correlation between *MTOR* mutation (LOT 1, 2, 5, 6) and lower mTORC1 activity (LOT 1, 2, 6 and 7). Specifically, 3/4 cases with *MTOR* mutations had lower levels of mTORC1 activation (LOT 1, 2, 6). One potential explanation for the moderate p-S6 and p-4E-BP1 activation levels in these cases may be the presence of a wild-type *MTOR* allele and protein, in particular since mTORC1 dimerizes. NGS and Sanger studies were consistent with the presence of a wild-type *MTOR* allele suggesting that mutations were heterozygous. Furthermore, copy number analyses available for 3 out of the 4 cases (a normal sample is

Author Manuscript Author Manuscript Author Manuscript Author Manuscript

missing for LOT 6) showed two copies of chromosome 1, where *MTOR* is located (1p36.22) (Supplementary Figure 6). mTOR forms a dimer with two interfaces between N-heat and M-heat domains. In the apo structure, the N-heat domain is positioned in a relatively open state with respect to the rest of the protein (Figure 2C left). Upon RHEB binding, the N-heat domain rotates toward the intersection of the M-heat and FAT domains, and the kinase catalytic cleft closes to align active site residues for catalysis[48,51]. This rotation approximates the dimer interaction surfaces (Figure 2C right). The changes induced by RHEB binding are not compatible with a mixed dimer of activated and inactivated mTOR[48]. Furthermore, RHEB-induced kinase activation is cooperative in the wild-type complex[48]. In the absence of RHEB, mTOR could adopt a heterogenous mixture of activation states depending upon whether it is constituted by wild-type dimers, heterodimers (of wild-type and mutant) or mutant dimers. Thus, the presence of a wild-type subunit could potentially reduce the impact of hyperactivating mTOR mutations. The overall mTORC1 activation state as compared, for instance, to tumors in which mTORC1 activation is driven by a single mutant protein (with loss of the wild-type allele) or by activation upstream (such as through *RHEB* or *TSC1/TSC2* mutations) may be reduced.

To extend the findings in our cohort, we reviewed all tumors categorized as chRCC-eo in the TCGA (KICH) project[52]. We used the NIH GDC Data Portal to review digital slides (www.portal.gdc.cancer.gov). While IHCs are unavailable (CK7+/CD117− status could not be confirmed), 4 out of 19 tumors morphologically resembled LOT (TCGA-KN-8437, TCGA-KM-8439, TCGA-KM-8441, TCGA-KM-8639). We assessed the mutation status of mTORC1 pathway genes in these 4 tumors. Interestingly, 2 of these tumors had pathogenic mTOR mutations (TCGA-KN-8437; p.L2427R and TCGA-KM-8441; p.I2017T) (Supplementary Figure 7A–B). TCGA-KN-8437 had a mutation in the same residue as LOT 1 in our cohort and the particular substitution, L2427R, has been shown to be a gain of function mutation in the literature[18]. Similarly, the mTOR mutation in TCGA-KM-8441 (p.I2017T) has been previously reported in tumors and shown to induce kinase activity in vitro[53]. Both tumors were reported to be diploid and without chromosome 1 loss. A third TCGA tumor had a pathogenic frameshift TSC1 mutation (TCGA-KM-8639; p.R718Pf*3). No mutations were found in mTORC1 pathway genes in the fourth tumor.

Consistently, all LOTs cases in our cohort were diploid with all 22 autosome pairs (Figure 4). None of the cases showed iconic chromosomal alterations of other RCCs, such as multiple chromosomal losses, which typify chromophobe RCC, 3p loss in clear cell RCC, or gain of chromosome 7 and 17 as seen in papillary RCC.

We next asked how LOTs relate to other RCCs and performed gene expression analyses. Whole transcriptome data was available for 6 cases (LOT 1–2 from UTSW[23] and the 4 TCGA LOTs[52]). We compared the gene expression profiles with those from chRCC-eo (9 from UTSW including 1 RON-favor chRCC-eo[23] and 15 from TCGA[52]), classic chRCC (35 from UTSW[23] and 46 from TCGA[52]) and RO (33 from UTSW including 4 RON-favor RO[23]). In addition, normal kidney samples (60 from UTSW[23] and 24 from TCGA[52]) were included. We generated a t-distributed stochastic neighbor embedding (t-SNE) plot, which showed tight clustering of the LOT cases, away from RO, chRCC-eo, classic chRCC

Author Manuscript Author Manuscript Author Manuscript Author Manuscript

and normal kidney (Figure 5A). Intriguingly, LOT clustered away even from chRCC with mTORC1 pathway gene mutations (Figure 5A).

We then focused on chRCC-eo and LOT due to their morphologic similarity. We found 1674 differentially expressed genes (DEGs) between LOT and chRCC-eo tumor samples at a false discovery rate (FDR) ≤ 0.05 with an absolute log2 fold-change (LogFC) ≥1.5. A heatmap of these DEGs highlights the differences between LOT and chRCC-eo (Figure 5B). KEGG analysis of the DEGs between LOT and chRCC-eo samples identified 175 differentially enriched pathways (Figure 5C). Of particular interest, mTOR signaling, protein processing in endoplasmic reticulum, and MAPK signaling pathways were enriched in the LOT respective to chRCC-eo. Overall, these findings suggest that LOTs have a unique gene expression signature that sets them apart from other tumors.

Discussion

We report a comprehensive molecular profiling of a recently described renal tumor entity, low-grade oncocytic tumor (LOT) expanding our understanding of this novel disease[19,21]. Our results show that LOT can present in both syndromic and non-syndromic cases with uniform morphology and IHC features. LOT tumors have converging mutations in mTOR pathway genes and mTORC1 activation. Gene expression analyses show that LOT has a unique gene expression signature that differs from close morphologic mimics, chRCC-eo and RO.

Our results support and expand the morphologic and IHC features previously reported. In 2019, Trpkov et al[19] reported 28 distinct LOTs from four institutional archives. All tumors had consistent morphology characterized by tight nests of bland tumor cells with eosinophilic cytoplasm and were devoid of prominent nuclear membrane irregularities. Informatively, LOTs had a unique immunoprofile with CD117 negativity and diffuse CK7 reactivity. These findings were consistently observed in 7 additional cases reported by Guo et al[21] and in the 22 tumors in our series.

These initial studies reported LOTs to be single, and devoid of a syndromic association. One patient in our series had multiple bilateral LOTs and had a likely pathogenic germline *TSC1* mutation. TSC syndrome can have variable penetrance and a significant percent of cases have de novo mutations with no known family history. Individuals may have a mild phenotype, particularly when the *TSC1* gene is implicated[54]. However, it is quite likely that our LOT 3 patient had TSC as the same *TSC1* germline mutation has been reported in a 3-generation family with mild clinical TSC features[55]. All tumors seen in this patient were indistinguishable morphologically and by IHC from other LOTs in our series. A recent study similarly reported multifocal LOTs in TSC and in end stage renal disease (ESRD)[22]. None of our patients had ESRD. Similarly, previous studies of kidneys in TSC patients include cases that morphologically resemble LOT histologically and by IHC (CD117−/CK7+)[4,5]. These findings support that LOT can occur in both the sporadic and syndromic context. Although metastases have not been reported to date in LOT, as illustrated by the benefits seen in our LOT 3 patient, rapalogs may be considered for the management of multiple

Author Manuscript Author Manuscript Author Manuscript Author Manuscript

syndromic LOTs. This is further supported by the observation that at least in some contexts, mTOR pathway mutations are associated with rapalog responsivenes[56,57].

The classification of renal tumors is largely based on morphologic, and to a lesser extent, molecular features. LOT exhibits distinct but overlapping histologic features with chRCC-eo and RO. Using exome and transcriptome sequencing Joshi et al, identified two main subtypes of RO. Type 1 tumors were diploid and exhibited *CCND1* rearrangement. In contrast, Type 2 tumors were hypodiploid with loss of chromosome 1, X/Y, and/or 14 and 21[41]. Type 2 tumors could progress to chRCC-eo[41]. Our prior work shows that most chRCC-eo are similar to RO, do not have classic chromosomal abnormalities of chRCC, and are often diploid[23]. In the TCGA dataset, 10/19 chRCC-eo showed the characteristic chRCC copy number pattern with loss of one copy of entire chromosomes for most chromosomes including 1, 2, 6, 10, 13, 17. In a Swiss cohort, chromosomal losses were observed in 27% of chRCC-eo[58]. Our data and those from others[59] suggest that LOT, like RO and chRCC-eo, are largely diploid and lack the recurrent chromosomal abnormalities of classic chRCC. It is unclear, however, whether LOT is part of the spectrum of chRCC-eo and oncocytoma (RO). It is tempting to speculate a stepwise progression from RO (at least a subset) to chRCC-eo to classic chRCC especially given the link to chromosome 1 loss, which may be a driver event.

Our gene expression analyses show that LOTs have a unique expression profile that distinguishes these tumors from RO and chRCC (both classic and eosinophilic variant). These changes in gene expression likely contribute to differential protein expression (CK7, CD117). Other markers include FOXI1, which is expressed in chRCC-eo and not in LOT[60]. Both CD117 and FOXI1 are expressed in renal intercalated cells of distal tubules, suggesting perhaps that these cells give raise to chRCC-eo but not LOT. In fact, differences in the expression of FOXI1 mRNA in TCGA-pan RCC data allowed Tong K et al.[60] to identify 5 outlier cases in TCGA (4 of which are the same that we found to resemble LOT morphologically and one additional TCGA-MH-A857 from KIRP) which they reclassified as “eosinophilic chromophobe-like renal tumors”. Similarly, Skala SL et al.[61] found 2 out of their 10 institutional chRCC-eo to have low or absent FOXI1 expression. The morphology of these 2 tumors matches LOT and they were reported to have *MTOR* mutations, were diploid, and lacked chromosome 1 loss (Supplementary Figure 7A–B).

Our study illustrates that LOT have converging mutations in genes involved in the mTORC1 pathway (*MTOR, TSC1* and *RHEB*). Interestingly, using target gene sequencing, Tjota et al. recently described a spectrum of renal tumors with pathogenic mutations in *TSC1/TSC2/MTOR*.[59,62] A subset of these tumors (group 2) were CK7+ and had absent to weak (1+) CD117 expression and could represent LOT. Though it may be tempting to classify LOT as “TSC/mTOR-associated renal neoplasms”[62], these represent a heterogenous group of tumors based on morphology and IHC. Somatic alterations in mTOR pathway genes have been described in several RCC[23,52,61–65]. We first reported the identification of mTORC1 pathway gene mutations in ccRCC in 2011, when we found mutations in *TSC1*[66]. Subsequently, mTORC1 pathway gene mutations were reported in chRCC by us and others[23,52,59,61]. mTORC1 pathway mutations have also been reported in eosinophilic tumors including EVT and ESC RCC[2]. Thus, mTORC1 pathway mutations alone are not a sufficiently distinguishing feature.

Author Manuscript Author Manuscript Author Manuscript Author Manuscript

In our cohort, all cases exhibited activation of mTORC1. mTOR is found in two complexes, mTORC1 and mTORC2. Our data suggest that mTORC1 may, in particular, be affected. This idea is supported by the finding of mTORC1 activation (of which p-S6 and p-4EBP1 are specific markers), as well as by mutations in *TSC1* and *RHEB*, that specifically regulate mTORC1. The TSC complex is a heterotrimer that includes TSC1 and TSC2 as well as TBC1D7 and acts as a GTPase activating protein (GAP) for the small GTPase RHEB[67]. TSC complex inactivation leads to constitutive activation of RHEB. In its GTP-bound form, RHEB binds and activates mTORC1. mTORC1 plays a central role in coordinating cell growth and metabolism by taking cues from its environment such as availability of nutrients and growth factors[67]. For a cell to divide, it needs to promote anabolism and increase its mass. mTORC1 is a downstream mediator of several growth factors and mitogen-dependent signaling pathways that converge in the regulation of the TSC complex.

In our LOT cases, the levels of mTORC1 activation varied. Interestingly, we noted a correlation between LOT cases with mTOR mutations and lower mTORC1 activation. A potential explanation for this finding is that *MTOR* mutations were heterozygous and the wild-type allele appeared to be preserved. The significance of a preserved wild-type protein may be heightened by the fact that mTORC1 complexes are homodimers. This consideration is particularly interesting by comparison to EVT[14,17] where *MTOR* activating mutations are typically accompanied by loss of chromosome 1 (and the 2nd copy of *MTOR*). This may contribute to explain the higher grade appearance of EVT compared to LOT. One possibility is that LOT may evolve to EVT upon loss of chromosome 1 (and the remaining *MTOR* wild-type allele). Thus, mTORC1 may serve as rheostat in LOT, EVT, as well as other tumors with driver mTORC1 pathway alterations and morphologic overlap such as ESC-RCC. Provocatively, and as shown in Supplementary Figure 2C–F, LOT 3 and LOT 4 showed focal distinct area that morphologically resembled EVT/chRCC-eo with stronger p-S6 expression (data not shown). Furthermore, mTORC1 pathway mutations appear to be associated with worse clinical outcomes in chRCC[68]. While this makes sense conceptually, most tumors described to date (and our own observations) do not show morphologic subclones suggestive of progression. As alluded to above, it is also possible that they involve different cells of origin. Thus, the extent to which these tumors are related remains to be fully determined.

In summary, our study provides a comprehensive molecular, and histopathologic analysis of low grade oncocytic tumors, a recently described renal cell neoplasm. We show that they exhibit a unique gene expression signature that distinguishes them from morphologically related tumors, as well as consistent mTORC1 pathway mutations and broaden the clinical presentation to include syndromic patients. Our data supports LOT as a unique and distinct entity of indolent clinical behavior.

Supplementary Material

Refer to Web version on PubMed Central for supplementary material.

Author Manuscript Author Manuscript Author Manuscript Author Manuscript

Acknowledgments:

We acknowledge the patients whose samples provided the foundation for this study and are grateful to the Kidney Cancer Program and the Clinical Data Warehouse teams for their support and assistance.

Funding Sources:

This work was supported by the NIH sponsored Kidney Cancer SPORE grant (P50CA196516) and endowment from Jan and Bob Pickens Distinguished Professorship in Medical Science and Brock Fund for Medical Science Chair in Pathology.

References

1. Trpkov K et al. New developments in existing WHO entities and evolving molecular concepts: The Genitourinary Pathology Society (GUPS) update on renal neoplasia. Mod Pathol 10.1038/s41379-021-00779-w (2021).
2. Trpkov K et al. Novel, emerging and provisional renal entities: The Genitourinary Pathology Society (GUPS) update on renal neoplasia. Mod Pathol 34, 1167–1184 (2021). [PubMed: 33526874]
3. Williamson SR et al. Diagnostic criteria for oncocytic renal neoplasms: a survey of urologic pathologists. Hum Pathol 63, 149–156 (2017). [PubMed: 28315424]
4. Guo J et al. Tuberous sclerosis-associated renal cell carcinoma: a clinicopathologic study of 57 separate carcinomas in 18 patients. Am J Surg Pathol 38, 1457–1467 (2014). [PubMed: 25093518]
5. Yang P et al. Renal cell carcinoma in tuberous sclerosis complex. Am J Surg Pathol 38, 895–909 (2014). [PubMed: 24832166]
6. Pavlovich CP et al. Renal tumors in the Birt-Hogg-Dube syndrome. Am J Surg Pathol 26, 1542–1552 (2002). [PubMed: 12459621]
7. McKenney JK, Przybycin CG, Trpkov K & Magi-Galluzzi C Eosinophilic solid and cystic renal cell carcinomas have metastatic potential. Histopathology 72, 1066–1067 (2018). [PubMed: 29265482]
8. Trpkov K et al. Eosinophilic Solid and Cystic Renal Cell Carcinoma (ESC RCC): Further Morphologic and Molecular Characterization of ESC RCC as a Distinct Entity. Am J Surg Pathol 41, 1299–1308 (2017). [PubMed: 28786877]
9. Trpkov K et al. Eosinophilic, Solid, and Cystic Renal Cell Carcinoma: Clinicopathologic Study of 16 Unique, Sporadic Neoplasms Occurring in Women. Am J Surg Pathol 40, 60–71 (2016). [PubMed: 26414221]
10. Argani P MiT family translocation renal cell carcinoma. Semin Diagn Pathol 32, 103–113 (2015). [PubMed: 25758327]
11. Srigley JR et al. The International Society of Urological Pathology (ISUP) Vancouver Classification of Renal Neoplasia. Am J Surg Pathol 37, 1469–1489 (2013). [PubMed: 24025519]
12. Gill AJ et al. Succinate dehydrogenase (SDH)-deficient renal carcinoma: a morphologically distinct entity: a clinicopathologic series of 36 tumors from 27 patients. Am J Surg Pathol 38, 1588–1602 (2014). [PubMed: 25025441]
13. Smith SC et al. A distinctive, low-grade oncocytic fumarate hydratase-deficient renal cell carcinoma, morphologically reminiscent of succinate dehydrogenase-deficient renal cell carcinoma. Histopathology 71, 42–52 (2017). [PubMed: 28165631]
14. Trpkov K et al. High-grade oncocytic tumour (HOT) of kidney in a patient with tuberous sclerosis complex. Histopathology 75, 440–442 (2019). [PubMed: 31002177]
15. He H et al. “High-grade oncocytic renal tumor”: morphologic, immunohistochemical, and molecular genetic study of 14 cases. Virchows Arch 473, 725–738 (2018). [PubMed: 30232607]
16. Chen YB et al. Somatic Mutations of TSC2 or MTOR Characterize a Morphologically Distinct Subset of Sporadic Renal Cell Carcinoma With Eosinophilic and Vacuolated Cytoplasm. Am J Surg Pathol 43, 121–131 (2019). [PubMed: 30303819]
17. Kapur P et al. Eosinophilic Vacuolated Tumor of the Kidney: A Review of Evolving Concepts in This Novel Subtype With Additional Insights From a Case With MTOR Mutation and Concomitant Chromosome 1 Loss. Adv Anat Pathol 10.1097/PAP.0000000000000299 (2021).

Author Manuscript Author Manuscript Author Manuscript Author Manuscript

18. Chen YB et al. Molecular analysis of aggressive renal cell carcinoma with unclassified histology reveals distinct subsets. Nat Commun 7, 13131 (2016). [PubMed: 27713405]
19. Trpkov K et al. Low-grade oncocytic tumour of kidney (CD117-negative, cytokeratin 7-positive): a distinct entity? Histopathology 75, 174–184 (2019). [PubMed: 30895640]
20. Siadat F & Trpkov K ESC, ALK, HOT and LOT: Three Letter Acronyms of Emerging Renal Entities Knocking on the Door of the WHO Classification. Cancers (Basel) 12 (2020).
21. Guo Q et al. Characterization of a distinct low-grade oncocytic renal tumor (CD117-negative and cytokeratin 7-positive) based on a tertiary oncology center experience: the new evidence from China. Virchows Arch 10.1007/s00428-020-02927-0 (2020).
22. Kravtsov O et al. Low-Grade Oncocytic Tumor of Kidney (CK7-Positive, CD117-Negative): Incidence in a Single Institutional Experience with Clinicopathological and Molecular Characteristics. Hum Pathol 10.1016/j.humpath.2021.04.013 (2021).
23. Durinck S et al. Spectrum of diverse genomic alterations define non-clear cell renal carcinoma subtypes. Nat Genet 47, 13–21 (2015). [PubMed: 25401301]
24. Trpkov K & Hes O New and emerging renal entities: a perspective post-WHO 2016 classification. Histopathology 74, 31–59 (2019). [PubMed: 30565301]
25. Pena-Llopis S & Brugarolas J Simultaneous isolation of high-quality DNA, RNA, miRNA and proteins from tissues for genomic applications. Nat Protoc 8, 2240–2255 (2013). [PubMed: 24136348]
26. Li H & Durbin R Fast and accurate short read alignment with Burrows-Wheeler transform. Bioinformatics 25, 1754–1760 (2009). [PubMed: 19451168]
27. DePristo MA et al. A framework for variation discovery and genotyping using next-generation DNA sequencing data. Nat Genet 43, 491–498 (2011). [PubMed: 21478889]
28. McKenna A et al. The Genome Analysis Toolkit: a MapReduce framework for analyzing next-generation DNA sequencing data. Genome Res 20, 1297–1303 (2010). [PubMed: 20644199]
29. Van der Auwera GA et al. From FastQ data to high confidence variant calls: the Genome Analysis Toolkit best practices pipeline. Curr Protoc Bioinformatics 43, 11 10 11–33 (2013).
30. Cibulskis K et al. Sensitive detection of somatic point mutations in impure and heterogeneous cancer samples. Nat Biotechnol 31, 213–219 (2013). [PubMed: 23396013]
31. Koboldt DC et al. VarScan 2: somatic mutation and copy number alteration discovery in cancer by exome sequencing. Genome Res 22, 568–576 (2012). [PubMed: 22300766]
32. Hansen NF, Gartner JJ, Mei L, Samuels Y & Mullikin JC Shimmer: detection of genetic alterations in tumors using next-generation sequence data. Bioinformatics 29, 1498–1503 (2013). [PubMed: 23620360]
33. Chiang C et al. SpeedSeq: ultra-fast personal genome analysis and interpretation. Nat Methods 12, 966–968 (2015). [PubMed: 26258291]
34. Saunders CT et al. Strelka: accurate somatic small-variant calling from sequenced tumor-normal sample pairs. Bioinformatics 28, 1811–1817 (2012). [PubMed: 22581179]
35. Wang K, Li M & Hakonarson H ANNOVAR: functional annotation of genetic variants from high-throughput sequencing data. Nucleic Acids Res 38, e164 (2010). [PubMed: 20601685]
36. Wang T et al. Probability of phenotypically detectable protein damage by ENU-induced mutations in the Mutagenetix database. Nat Commun 9, 441 (2018). [PubMed: 29382827]
37. Talevich E, Shain AH, Botton T & Bastian BC CNVkit: Genome-Wide Copy Number Detection and Visualization from Targeted DNA Sequencing. PLoS Comput Biol 12, e1004873 (2016). [PubMed: 27100738]
38. Turajlic S et al. Deterministic Evolutionary Trajectories Influence Primary Tumor Growth: TRACERx Renal. Cell 173, 595–610 e511 (2018). [PubMed: 29656894]
39. Dobin A et al. STAR: ultrafast universal RNA-seq aligner. Bioinformatics 29, 15–21 (2013). [PubMed: 23104886]
40. Liao Y, Smyth GK & Shi W featureCounts: an efficient general purpose program for assigning sequence reads to genomic features. Bioinformatics 30, 923–930 (2014). [PubMed: 24227677]
41. Joshi S et al. The Genomic Landscape of Renal Oncocytoma Identifies a Metabolic Barrier to Tumorigenesis. Cell Rep 13, 1895–1908 (2015). [PubMed: 26655904]

Author Manuscript Author Manuscript Author Manuscript Author Manuscript

42. Robinson MD, McCarthy DJ & Smyth GK edgeR: a Bioconductor package for differential expression analysis of digital gene expression data. Bioinformatics 26, 139–140 (2010). [PubMed: 19910308]
43. Robinson MD & Oshlack A A scaling normalization method for differential expression analysis of RNA-seq data. Genome Biol 11, R25 (2010). [PubMed: 20196867]
44. Johnson WE, Li C & Rabinovic A Adjusting batch effects in microarray expression data using empirical Bayes methods. Biostatistics 8, 118–127 (2007). [PubMed: 16632515]
45. Zhao S et al. A brain somatic RHEB doublet mutation causes focal cortical dysplasia type II. Exp Mol Med 51, 84 (2019). [PubMed: 31337748]
46. Xu J et al. Mechanistically distinct cancer-associated mTOR activation clusters predict sensitivity to rapamycin. J Clin Invest 126, 3526–3540 (2016). [PubMed: 27482884]
47. Lim JS et al. Brain somatic mutations in MTOR cause focal cortical dysplasia type II leading to intractable epilepsy. Nat Med 21, 395–400 (2015). [PubMed: 25799227]
48. Yang H et al. Mechanisms of mTORC1 activation by RHEB and inhibition by PRAS40. Nature 552, 368–373 (2017). [PubMed: 29236692]
49. Wagle N et al. Activating mTOR mutations in a patient with an extraordinary response on a phase I trial of everolimus and pazopanib. Cancer Discov 4, 546–553 (2014). [PubMed: 24625776]
50. Ghosh AP et al. Point mutations of the mTOR-RHEB pathway in renal cell carcinoma. Oncotarget 6, 17895–17910 (2015). [PubMed: 26255626]
51. Yang H et al. mTOR kinase structure, mechanism and regulation. Nature 497, 217–223 (2013). [PubMed: 23636326]
52. Davis CF et al. The somatic genomic landscape of chromophobe renal cell carcinoma. Cancer Cell 26, 319–330 (2014). [PubMed: 25155756]
53. Ohne Y et al. Isolation of hyperactive mutants of mammalian target of rapamycin. J Biol Chem 283, 31861–31870 (2008). [PubMed: 18812319]
54. Au KS et al. Genotype/phenotype correlation in 325 individuals referred for a diagnosis of tuberous sclerosis complex in the United States. Genet Med 9, 88–100 (2007). [PubMed: 17304050]
55. Streff H et al. TSC1 Variant Associated With Mild or Absent Clinical Features of Tuberous Sclerosis Complex in a Three-Generation Family. Pediatr Neurol 110, 89–91 (2020). [PubMed: 32654957]
56. Wolff N et al. Sirolimus and temsirolimus for epithelioid angiomyolipoma. J Clin Oncol 28, e65–68 (2010). [PubMed: 20048172]
57. Maroto P et al. Biallelic TSC2 Mutations in a Patient With Chromophobe Renal Cell Carcinoma Showing Extraordinary Response to Temsirolimus. J Natl Compr Canc Netw 16, 352–358 (2018). [PubMed: 29632054]
58. Ohashi R et al. Classic Chromophobe Renal Cell Carcinoma Incur a Larger Number of Chromosomal Losses Than Seen in the Eosinophilic Subtype. Cancers (Basel) 11 (2019).
59. Tjota MY, Wanjari P, Segal J & Antic T TSC/MTOR mutated eosinophilic renal tumors are a distinct entity that are CK7+/CK20-/vimentin-: a validation study. Hum Pathol 10.1016/j.humpath.2020.12.006 (2020).
60. Tong K & Hu Z FOXI1 expression in chromophobe renal cell carcinoma and renal oncocytoma: a study of The Cancer Genome Atlas transcriptome-based outlier mining and immunohistochemistry. Virchows Arch 10.1007/s00428-020-02900-x (2020).
61. Skala SL et al. Next-generation RNA Sequencing-based Biomarker Characterization of Chromophobe Renal Cell Carcinoma and Related Oncocytic Neoplasms. Eur Urol 78, 63–74 (2020). [PubMed: 32299640]
62. Tjota M et al. Eosinophilic Renal Cell Tumors With a TSC and MTOR Gene Mutations Are Morphologically and Immunohistochemically Heterogenous: Clinicopathologic and Molecular Study. Am J Surg Pathol 44, 943–954 (2020). [PubMed: 32091432]
63. Ricketts CJ et al. The Cancer Genome Atlas Comprehensive Molecular Characterization of Renal Cell Carcinoma. Cell Rep 23, 313–326 e315 (2018). [PubMed: 29617669]

Author Manuscript Author Manuscript Author Manuscript Author Manuscript

64. Cancer Genome Atlas Research, N. Comprehensive molecular characterization of clear cell renal cell carcinoma. Nature 499, 43–49 (2013). [PubMed: 23792563]

65. Linehan WM & Ricketts CJ The Cancer Genome Atlas of renal cell carcinoma: findings and clinical implications. Nat Rev Urol 16, 539–552 (2019). [PubMed: 31278395]

66. Kucejova B et al. Interplay between pVHL and mTORC1 pathways in clear-cell renal cell carcinoma. Mol Cancer Res 9, 1255–1265 (2011). [PubMed: 21798997]

67. Saxton RA & Sabatini DM mTOR Signaling in Growth, Metabolism, and Disease. Cell 168, 960–976 (2017). [PubMed: 28283069]

68. Roldan-Romero JM et al. Molecular characterization of chromophobe renal cell carcinoma reveals mTOR pathway alterations in patients with poor outcome. Mod Pathol 33, 2580–2590 (2020). [PubMed: 32616874]

Author Manuscript Author Manuscript Author Manuscript Author Manuscript

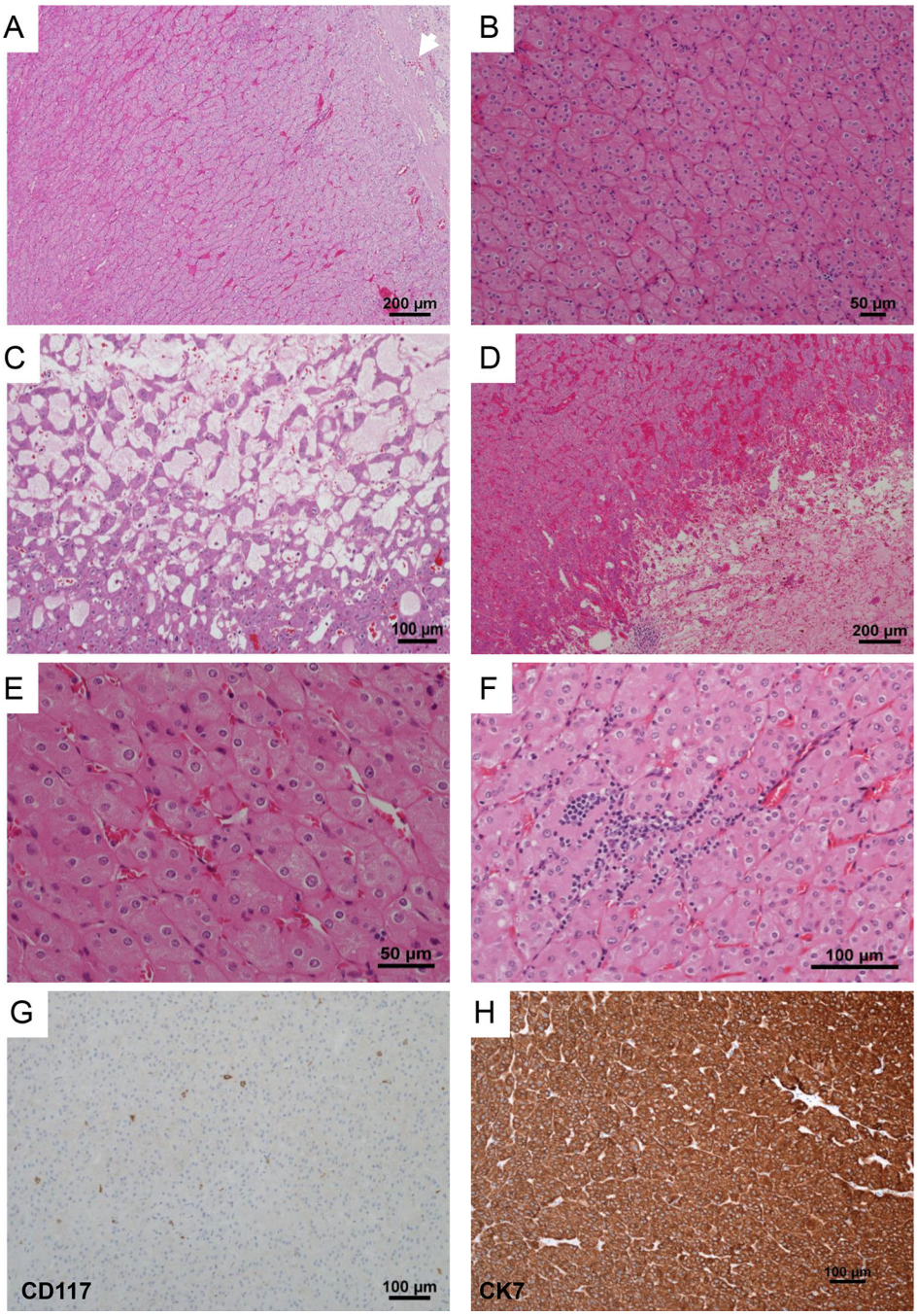

Figure 1. Histologic characteristics of LOT.

Representative H&E images from LOT reveal a well circumscribed partly encapsulated eosinophilic tumor (white arrow) (A) composed of homogenous cells arranged in sheets of tight nests (B) with focal edematous areas with loose cords of tumor cells (C), and occasional dilated vascular channels and hemorrhage (D). High-power images show that the tumors are uniformly composed of cells with abundant finely granular eosinophilic cytoplasm, indistinct cell borders, round nuclei with relatively smooth membranes, subtle perinuclear clearing and binucleation (E). Lymphoid clusters are frequent (F).

Author Manuscript Author Manuscript Author Manuscript Author Manuscript

Representative immunohistochemical profile of CD117 with only scattered positive mast cells (G), and cytokeratin 7, which is strong and diffusely positive (H).

Author Manuscript Author Manuscript Author Manuscript Author Manuscript

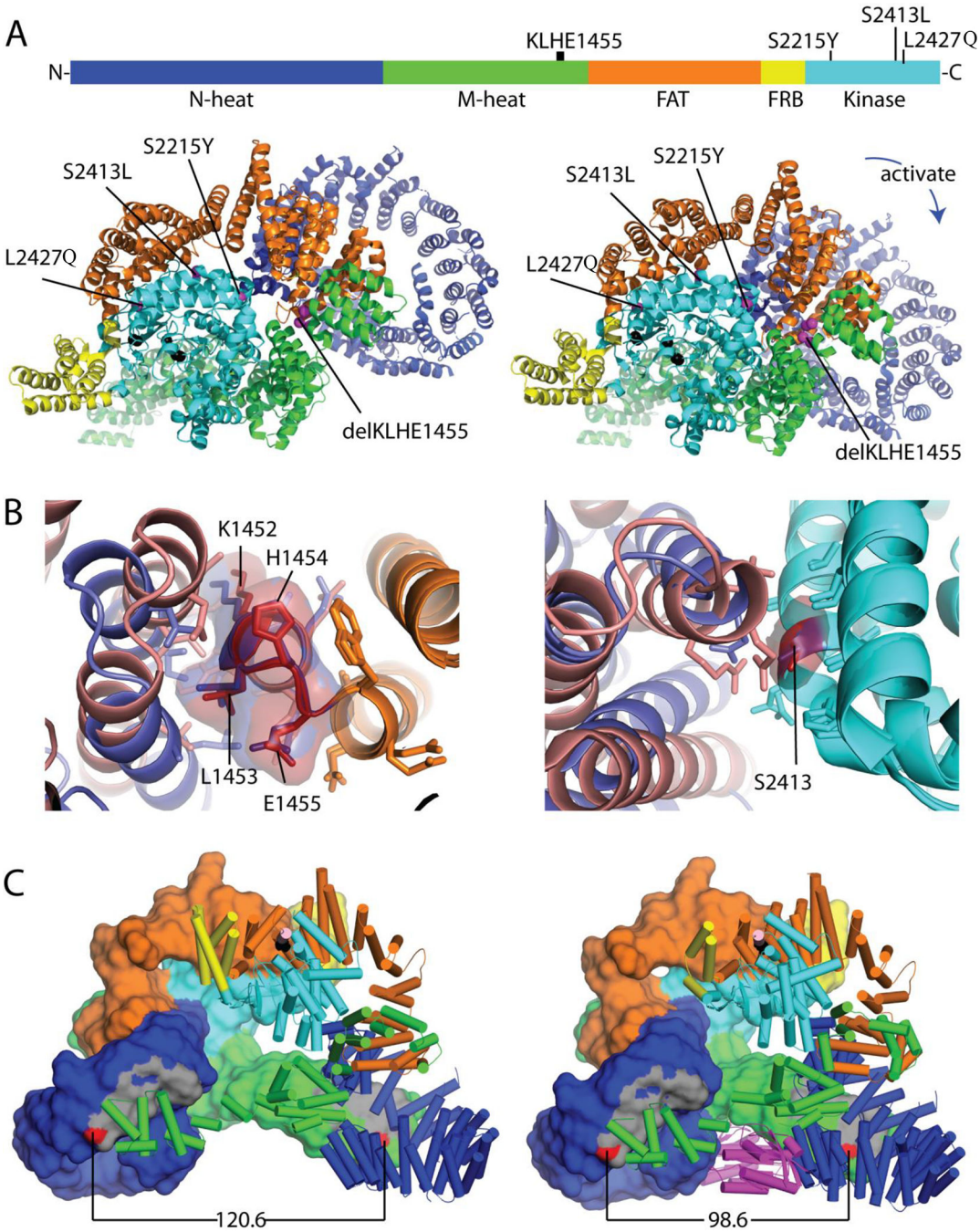

Figure 2. Schematic mapping of mTOR mutations in LOT samples.

(A) Mutation positions in the mTOR protein primary structure as well as tertiary structures of apo mTORC1 (PDB: 6bcx, left) and RHEB-activated mTORC1 (PDB: 6bcu, right) with colored domains. (B) Structure context of less well characterized mTOR mutations. Left: Superimposed wild type mTOR FAT domain hinge region (orange) with area corresponding to K1452-E1455 (deleted in LOT 6) illustrating differential interactions with neighboring FAT helices in apo (slate) and RHEB activated (salmon) conformations. Residues within 4Å are in stick. Right: Superimposed kinase C-lobes (cyan) containing the S2413I mutation

Author Manuscript Author Manuscript Author Manuscript Author Manuscript

(LOT 5). The mutation is positioned at the FAT domain interface, which adopts alternate conformations in the active (salmon) and apo (slate) states. Residues within 4Å are in stick. (C) mTORC1 dimerization interface is incompatible with mixed dimers. Left: mTOR dimer (domains colored as above) from an apo mTORC1 structure (PDB: 6BCX) with one chain in surface rendering and the second chain in cartoon mode. The dimer interface (gray) is formed by interaction of N-heat (dark blue) and M-heat domains (green), with the distance between two residues in the dimer interface (N612 and R1161, red) indicated below. Right: RHEB (magenta)-activated mTOR dimer with closer interaction surfaces as shown by the distance between N612 and R1161 (red).

Author Manuscript Author Manuscript Author Manuscript Author Manuscript

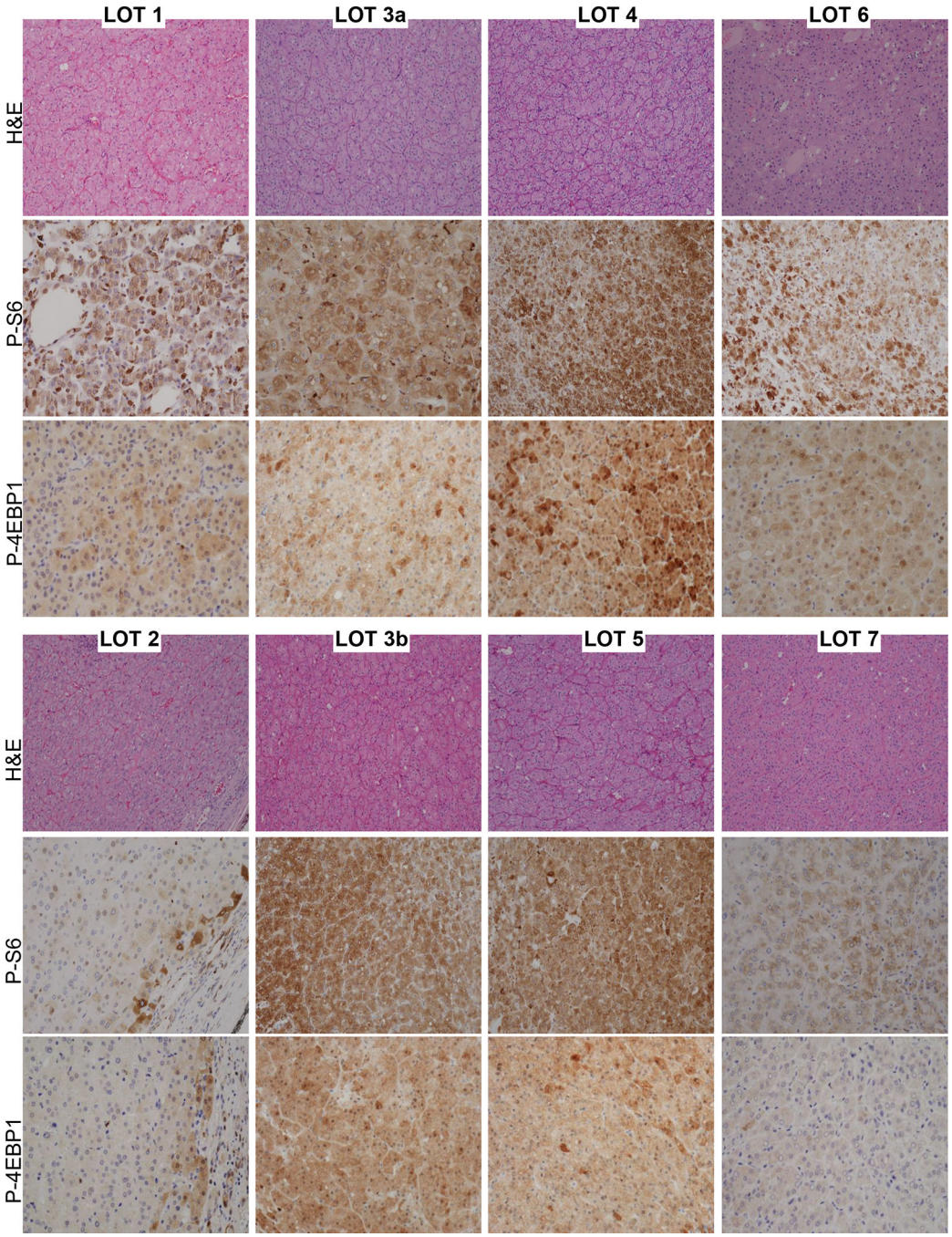

Figure 3. Evaluation of mTORC1 pathway activation in LOT.

Representative H&E, p-S6, and p-4EBP1 immunohistochemical expression in LOTs. The percentage of tumor cells expressing cytoplasmic phospho-S6 and the intensity of expression is tabulated in the Table 2.

Author Manuscript Author Manuscript Author Manuscript Author Manuscript

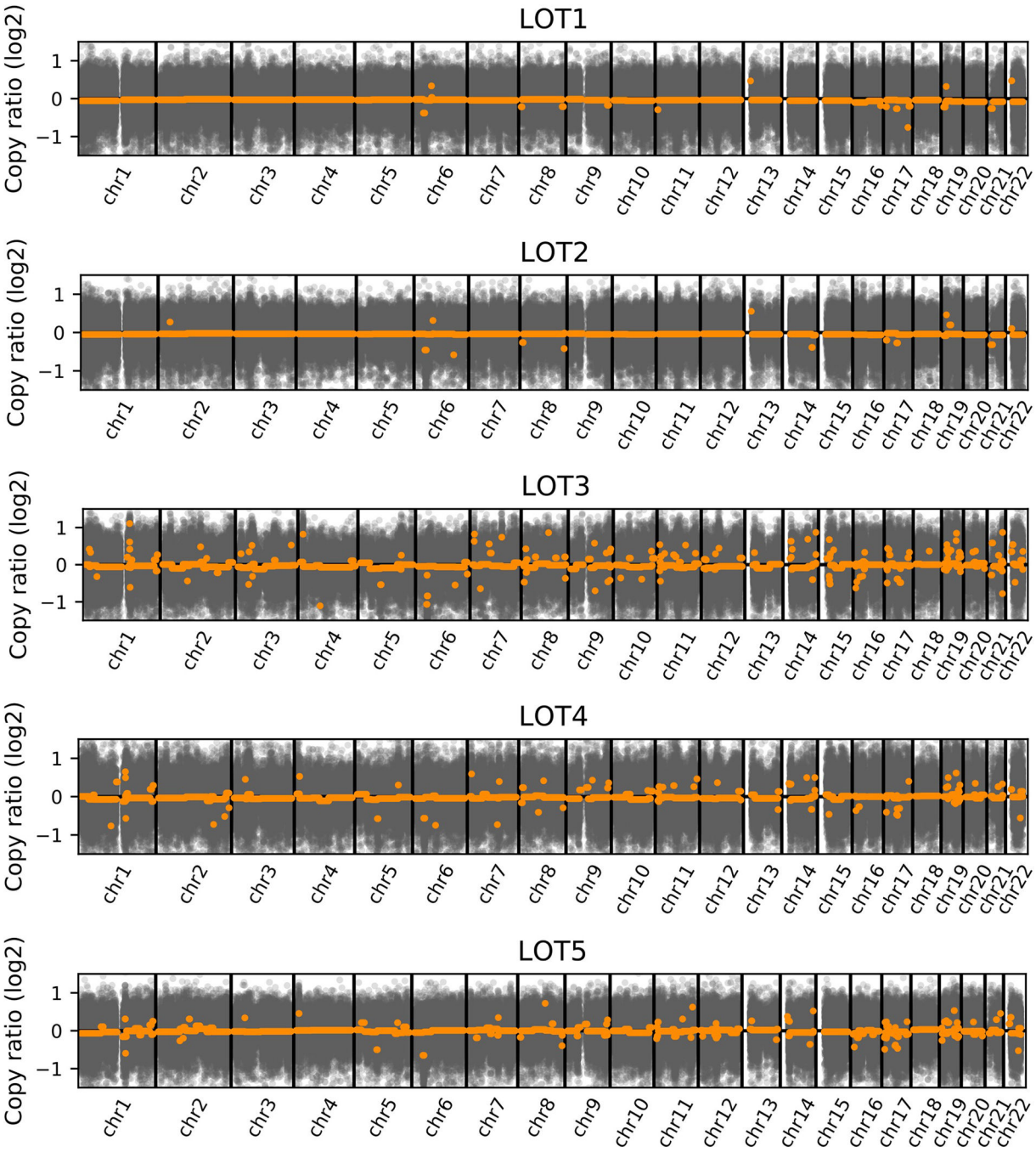

Figure 4. Copy number analysis in LOT.

Whole-genome profiles of $\log_2$ copy ratio by CNVkit on WES in LOTs. Average log2 copy ratio estimations are marked in orange.

Author Manuscript Author Manuscript Author Manuscript Author Manuscript

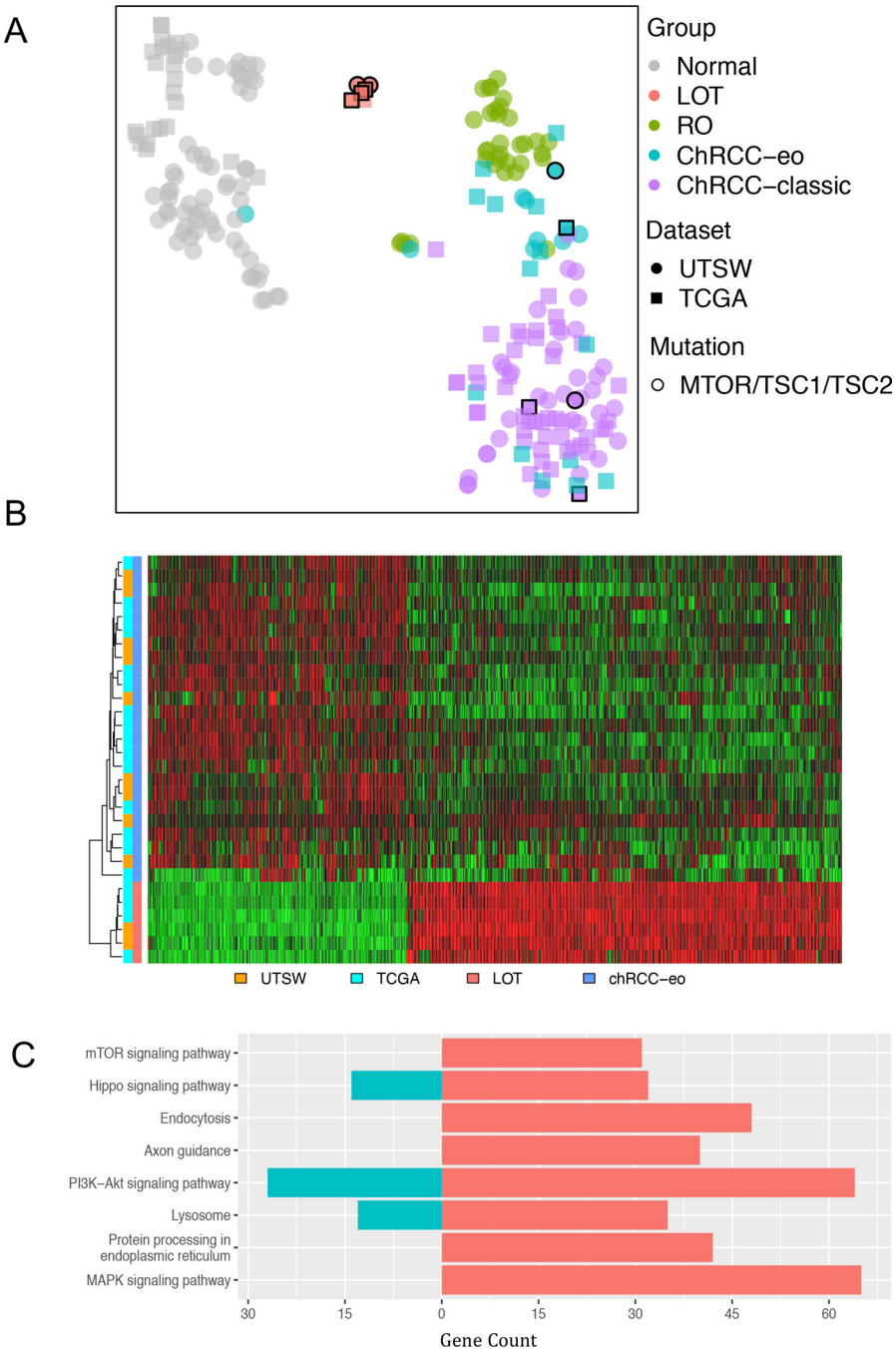

Figure 5. RNA-seq-based clustering of LOT, RO and chRCC.

(A) t-distributed stochastic neighbor embedding (t-SNE) plot of filtered whole transcriptomic data from pooled UTSW and TCGA cohorts showing clustering of LOT samples away from classic chRCC, chRCC-eo, and RO, including chRCC with mTORC1 pathway gene mutations (highlighted with black borders). (B) Heatmap of 1674 most differentially expressed genes distinguishing LOT from chRCC-eo. (C) Select enriched

pathways between LOT and chRCC-eo by KEGG analysis of DEGs with over-representation p-value ≤0.05. Up (red) and down (cyan) regulated gene counts are shown.

Author Manuscript Author Manuscript Author Manuscript Author Manuscript

Author Manuscript Author Manuscript Author Manuscript Author Manuscript

Table 1.

Clinicopathologic Characteristics of LOT Cases in the Cohort

Patient ID	Age	Sex	Presentation	Family History	Other Significant Medical History	Original Diagnosis	Nephrectomy	Laterality	Tumor Size (cm)	Focality (number)	pT	pN	Stage	Metastasis	Follow-up (months)
LOT 1	79	F	Back pain	None	Contralateral metastatic ccRCC	ChRCC-eo	Partial	Right	7.8	Unifocal	pT2a	pNx	II	No	Deceased (26)
LOT 2	86	F	Incidental	None	None	ChRCC-eo	Radical	Right	6.5	Unifocal	pT1b	pNx	I	No	ALF (3)
LOT 3a	63	F	Anemia	Father with b/l Nx for unknown reason	B/l multiple LOTs	ChRCC-eo	Partial	Right	4.0, 2.3, 1.5, 1.4, 0.8, 0.5	Multifocal (6)	pT1a *	pNx	I	No	ALF (37)
LOT 3b						ChRCC-eo	Partial	Left	5.3, 5.2, 4.9, 3.7, 2.1, 2.0, 1.9, 1.6, 1.0, 0.9	Multifocal (10)	pT1b *	pNx	I	No	
LOT 4	69	M	Hematuria	None	None	ChRCC-eo	Partial	Right	2.3	Unifocal	pT1a	pNx	I	No	ALF (29)
LOT 5	71	F	Incidental	None	Prior contralateral nephrectomy for benign tumor	ChRCC-eo	Partial	Right	3.8	Unifocal	pT1a	pNx	I	No	ALF (53)
LOT 6	75	F	Incidental	None	None	ChRCC-eo	Partial	Left	2.4	Unifocal	pT1a	pNx	I	No	Deceased (36)
LOT 7	84	M	Incidental	None	Contralateral renal mass followed with AS	ChRCC-eo	Radical	Right	6.5	Unifocal	pT1b	pNx	I	No	Deceased (29)

ccRCC: clear cell renal cell carcinoma; B/l: bilateral; Nx: nephrectomy; AS: active surveillance; ChRCC-eo: chromophobe renal cell carcinoma, eosinophilic variant

*: pT represents the highest stage

ALF: alive at last follow-up.

Author Manuscript Author Manuscript Author Manuscript Author Manuscript

Table 2.

Immunohistochemical Profile of LOT Cases in the Cohort

Patient ID	CD117	CK7	P-S6		P-4EBP1	
			intensity	percentage	intensity	percentage
LOT 1	negative	diffuse strong positive	moderate	20	weak-moderate	30
LOT 2	negative	diffuse strong positive	weak-moderate	5	weak-moderate	5
LOT 3a*	negative	diffuse strong positive	moderate-strong	90	weak-moderate	40
LOT 3b*	negative	diffuse strong positive	strong	90	moderate	60
LOT 4	negative	diffuse strong positive	strong	75	moderate	50
LOT 5	negative	diffuse strong positive	moderate	80	moderate	50
LOT 6	negative	diffuse strong positive	moderate	30	weak-moderate	20
LOT 7	negative	diffuse strong positive	weak-moderate	5	weak	5

*: Representative section from a total of 5 tumors were evaluated by immunohistochemistry.

Author Manuscript Author Manuscript Author Manuscript Author Manuscript

Table 3.

Alterations identified in LOT Cases in the Cohort

Genomic ID	Chromosome	Start Position	End Position	Reference Sequence	Tumor Sequence	Matched Normal Sequence	Gene	Variant_Classification	Validation_Method*	Somatic_Mutation*	Amino Acid Alteration
XP238T	chr1	11114338	11114338	A	T	A	*MTOR*	nonsynonymous SNV	Prior	NM_004958.3:c.7280 A>T	p.Leu2427Gln
17827T	chr1	11124516	11124516	G	T	G	*MTOR*	nonsynonymous SNV	Prior	NM_004958.3:c.6644G>T	p.Ser2215Tyr
KC02816-T1-FFPE	chr9	132902719	132902719	A	AGCTT	A	*TSC1*	frameshift substitution	Sangers	NM_000368.4:c.2273_2276dup	p.Arg760Serfs*2
KC02129-T1-FFPE	chr7	151490963	151490964	TA	AG	TA	*RHEB*	nonsynonymous SNV	Sangers	NM_005614.3:c.103_104delinsCT	p.Tyr35Leu
KC02942-T2-FFPE	chr1	11114380	11114381	CT	AG	CT	*MTOR*	nonsynonymous SNV	Sangers	NM_004958.3:c.7237_7238delinsCT	p.Ser2413Leu
KC00627-T1-FFPE	chr1	11157255	11157267	ACTCGTGCAGTTT	A	not available	*MTOR*	nonframeshift substitution	Sangers	NM_004958.3:c.4354_4365del	p.Lys1452_Glu1455del
Not pass quality check					not available	not available					

ation were confirmed by Sanger